

Conference Paper

Substitution of a Conventional Gas Turbine By a HT-PEMFC APU: Feasibility Study

Bruna Carolina Castro Pereira Araújo and Francisco Miguel Ribeiro Proença Brojo

Universidade da Beira Interior

Abstract

The aviation industry is increasing leading to a harmful environmental impact. APU is liable for 20% of airport ground-based emissions, 50% of aircraft maintenance costs and more than 5% of the daily fuel consumption [1]. Aware of this growing problem and its consequences, research should be conducted targeting new, non-polluting energy sources capable of meeting or even exceeding the aircraft's electrical needs. With this in mind, the main goal of this article was to analyze the feasibility of implementing a HT-PEMFC system as a more sustainable alternative for the gas turbine APU in an Airbus A320. The fuel used was methane which requires a fuel processor to convert it into hydrogen before entering the fuel cell. The maximum output work of this methane-supplied system is estimated at 250 kW. Therefore, a fuel processor and a fuel cell mathematical models were required. The two models along with the thermodynamic analysis were performed in MATLAB. The aims of this project were to evaluate fuel processing of methane and its conversion into electric energy through a fuel cell; to perform the thermodynamic analysis of HT-PEMFC APU based on the first and second laws of thermodynamics; and estimate the total weight, emissions and fuel consumption of the HT-PEMFC APU. The results of this research were very encouraging, as it shows that the breakeven weight of the HT-PEMFC, for a mass increment of 854 kg, was compensated by a fuel efficiency of ~ 2.7 times the conventional APU.

Keywords: APU, HT-PEMFC, Fuel cell

Corresponding Author:

Bruna Carolina Castro Pereira
 Araújo
 bruna_688@hotmail.com

Received: 26 November 2019

Accepted: 13 May 2020

Published: 2 June 2020

Publishing services provided by
Knowledge E

© Bruna Carolina Castro Pereira
 Araújo and Francisco Miguel
 Ribeiro Proença Brojo. This

article is distributed under the
 terms of the [Creative Commons](#)

[Attribution License](#), which

permits unrestricted use and
 redistribution provided that the
 original author and source are
 credited.

Selection and Peer-review under
 the responsibility of the
 ICEUBI2019 Conference
 Committee.

1. Introduction

The Auxiliary Power Unit (APU) is a self-contained unit responsible for providing electrical, pneumatic and hydraulic power to the aircraft, on the ground and during flight. The APU relies on ambient air and fuel from the engines to produce electrical power for aircraft systems and bleed air for air conditioning and engine start. A gas turbine is the conventional APU used in airplanes, favorable for its high power-to-weight ratio. The base design is a single-shaft gas turbine, powering an electrical generator and an air compressor, operating accordingly with the Brayton thermodynamic cycle.

OPEN ACCESS

Meanwhile, a fuel cell is an electrochemical device that combines fuel and an oxidant to produce electricity. The fuel is typically hydrogen which is supplied to the anode while the oxidant goes through the cathode, with water and heat as the by-products. A fuel cell APU is a stack of unit cells electrically connected in series to produce the desired voltage. The power density of the cells is a crucial parameter for aeronautical applications due to its relation to the weight of the stack. Higher power densities, normally, represent smaller and lighter stacks, however, it must be within the limits of current density. The conversion of chemical energy into electrical energy takes place without combustion occurring, so it is a highly efficient, clean, and quiet process. The High Temperature Proton Exchange Membrane Fuel Cell (HT-PEMFC) operates at temperatures of 120-200°C [2]. The higher operating temperatures increase reaction rates, prevent water management issues and provide a higher tolerance to poisons. HT-PEMFC systems no longer need to depend on hydrogen and instead, hydrocarbons or other low purity gases can serve as fuel, which is easier to produce onboard of an aircraft. Acid-doped polybenzimidazoles (PBI) membranes are likely the best candidate to an electrolyte for HT-PEMFCs, due to excellent thermal stability, low gas permeability and good proton transport above 150 °C even at low humidification conditions. Essentially, PBI- based membranes exhibit high proton conductivity when doped with strong acids such as phosphoric acid (H_3PO_4) [2].

The APU system is supplied with methane that needs to be reformed through a fuel processor before entering the fuel cell. Methane is converted into the reformat gas via two main reactions: methane steam reforming (MSR) and water gas shifting (WGS).

- MSR reaction is given as:



- WGS reaction is given as:



The Fuel Processor mathematical model is based on the total Gibbs free energy (G^T) to estimate the composition of the reformat and the flue gas. To convert the optimization problem to algebraic equations, Lagrange's undetermined method is used, and through an iterative process using the minimization tool in MATLAB, the minimum Gibbs free energy is determined and so are the equilibrium compositions.

- Gibbs minimization method

$$\min(G^t)_{T,P} = \min(\sum n_i G_i) = \min \left[\sum_i n_i \left(G_i^0 + RT \ln \frac{f_i}{f_i^0} \right) \right] \quad (3)$$

$$K_{MSR} = \frac{\dot{n}_{H_2} \dot{n}_{CO_2}}{\dot{n}_{CO} \dot{n}_{H_2O}} \quad (4)$$

$$K_{WGS} = \frac{\dot{n}_{H_2}^3 \dot{n}_{CO}}{\dot{n}_{CH_4} \dot{n}_{H_2O}} P_{tot}^2 \quad (5)$$

$$\ln K_{eq}(T) = \frac{-G^t}{RT} \quad (6)$$

K_{MSR} and K_{WGS} are the equilibrium constants of steam reforming and water gas shifting reactions, respectively. The equilibrium constants and the Gibbs minimization method are correlated by Equation 6. \dot{n}_i is the molar flow of the species i and P_{tot} is the pressure of the flow entering the reformer.

The HT-PEMFC mathematical model uses diffusion and electrochemical models. It is assumed single-phase, steady state, isothermal operation, one-dimensional electrochemical model. To calculate the concentration at catalyst surface Stefan Maxwell equation and the Fick's law are used and to determine the voltage and current density the electrochemical model is used.

- Stefan Maxwell model

- At anode

$$\frac{dX_{H_2O}}{dZ} = \frac{RT}{P} X_{H_2O} \left(\frac{\dot{n}_{H_2,g}}{D^{eff}_{H_2,H_2O}} \right) \quad (7)$$

$$\frac{dX_{CO_2}}{dZ} = \frac{RT}{P} X_{CO_2} \left(\frac{\dot{n}_{H_2,g}}{D^{eff}_{H_2,CO_2}} \right) \quad (8)$$

$$\frac{dX_{CO}}{dZ} = \frac{RT}{P} X_{CO} \left(\frac{\dot{n}_{H_2,g}}{D^{eff}_{H_2,CO}} \right) \quad (9)$$

$$\frac{dX_{CH_4}}{dZ} = \frac{RT}{P} X_{CH_4} \left(\frac{\dot{n}_{H_2,g}}{D^{eff}_{H_2,CH_4}} \right) \quad (10)$$

$$X_{H_2} = 1 - X_{H_2O} - X_{CO_2} - X_{CO} - X_{CH_4} \quad (11)$$

– At cathode

$$\frac{dX_{H_2O}}{dZ} = \frac{RT}{P} X_{H_2O} \left(\frac{\dot{n}_{O_2,g}}{D^{eff}_{H_2,H_2O}} \right) \quad (12)$$

$$\frac{dX_{N_2}}{dZ} = \frac{RT}{P} X_{N_2} \left(\frac{\dot{n}_{O_2,g}}{D^{eff}_{H_2,N_2}} \right) \quad (13)$$

$$X_{O_2} = 1 - X_{H_2O} - X_{N_2} \quad (14)$$

Where R is the universal gas constant, T is the stack temperature, P is the stack pressure, X is the molar fraction and the D^{eff} is the effective binary diffusion coefficient

• Fick's law model

$$\frac{\dot{n}_{H_2}}{S_{Pt,an}} = \frac{-D_{H_2}^{PA}(C_{H_2,Pt} - C_{H_2,dissolve})}{\delta_{an}} \quad (15)$$

$$C_{H_2,dissolve} = PX_{H_2}H_{H_2} \quad (16)$$

$$\frac{\dot{n}_{O_2}}{S_{Pt,ca}} = \frac{-D_{O_2}^{PA}(C_{O_2,Pt} - C_{O_2,dissolve})}{\delta_{ca}} \quad (17)$$

$$C_{O_2,dissolve} = PX_{O_2}H_{O_2} \quad (18)$$

Where R is the universal gas constant, S_{Pt} is the real surface area of Platinum (Pt) per geometric electrode area, D^{PA} is the diffusivity through, δ is the diffusivity through the ionomer, $C_{dissolve}$ is the equilibrium concentration in the acid film and can be found by the Henry's Law, as shown in Equation 16 and 18.

• Electrochemical Model

A reversible cell voltage (E_{rev}) is the voltage that can be obtained if the Gibbs free energy could be converted directly into electrical work without any losses. Practically, there are several irreversibilities within a fuel cell that causes the drop of the operating voltage. The difference between the theoretical voltage for the reaction and the actual cell voltage (V_{cell}) at a given current density is termed overpotential and is described in Equation 19. The prominent sources of overpotential in a fuel cell are: anode activation losses ($V_{act,an}$), cathode activation losses ($V_{act,ca}$) and ohmic resistance (V_{ohm}).

$$V_{cell} = E_{rev} - V_{act,an} - V_{act,ca} - V_{ohm} \quad (19)$$

$$E_{rev} = E^0 + \frac{RT}{ZF} \left[\frac{(RT)^{1.5} C_{H_2, Pt} - C_{O_2, Pt}^{0.5}}{a_{H_2O}} \right] \quad (20)$$

$$V_{act,an} = \frac{RT}{\alpha F} \sin^{-1} \left(\frac{i}{2i_{0,an}} \right) \quad (21)$$

$$V_{act,ca} = \frac{RT}{\alpha F} \sin^{-1} \left(\frac{i}{2i_{0,ca}} \right) \quad (22)$$

$$V_{ohm} = \frac{\sigma_m}{l_m} i \quad (23)$$

where z is the number of electrons transferred for each molecule of fuel, F denotes the Faraday constant, and E^0 is the ideal cell voltage at the fuel cell operating conditions, a_{H_2O} water activity, α is the charge transfer coefficient and i_0 is the exchange current density at the studied conditions per Pt unit area.

- Mass Balance

$$\sum \dot{m}_{in} = \sum \dot{m}_{out} \quad (24)$$

where \dot{m}_{in} is the mass flow entering the control volume and \dot{m}_{out} is the mass flow leaving the control volume.

- Energy Balance

$$\dot{Q}_{cv} - \dot{W}_{cv} + \sum \dot{m}_{in} h_{in} - \sum \dot{m}_{out} h_{out} = 0 \quad (25)$$

Where h represents the specific enthalpy, \dot{Q}_{cv} and \dot{W}_{cv} are the energy rates transfer by heat and by work, respectively, across the control surface.

- Entropy Balance

$$\sum \frac{\dot{Q}_{cv}}{T_{cv}} + \dot{S}_{gen} + \sum \dot{m}_{in} s_{in} - \sum \dot{m}_{out} s_{out} = 0 \quad (26)$$

Where s stands for specific entropy and \dot{S}_{gen} is the rate of entropy generated.

- Exergy Balance

$$\dot{E}x_{dest} = \sum \left(1 - \frac{T_0}{T_{cv}} \right) \dot{Q}_{cv} + \sum \dot{m}_{in} ex_{in} - \sum \dot{m}_{out} ex_{out} + \dot{E}x_w = 0 \quad (27)$$

$$ex = \sum X_i ex_{ch}^0 + RT_0 \sum X_i \ln X_i + (h - h_0) - T_0(s - s_0) \quad (28)$$

Where $\dot{E}x_{dest}$ is the rate of exergy destruction, $\dot{E}x_w$ is the exergy of work and T_0 is the temperature at reference conditions. The different forms of exergies, considered for this work, are physical exergy and chemical exergy and the total exergy is the sum of all these forms of exergy as presented in Eq. 28.

- First law efficiency

The electrical efficiency is defined as the ratio of the electrical power output from the APU system (\dot{W}_{APU}) divided by the lower heating value (LHV) of the fuel:

$$\eta_{ele} = \frac{\dot{W}_{APU}}{\dot{n}_{fuel} LHV_{fuel}} \quad (29)$$

The thermal efficiency of the APU system is defined as:

$$\eta_{thermal} = \frac{\sum \dot{Q}}{\dot{n}_{fuel} LHV_{fuel}} \quad (30)$$

The cogeneration efficiency of the fuel cell is defined as:

$$\eta_{cog} = \frac{\dot{W}_{APU} + \sum \dot{Q}}{\dot{n}_{fuel} LHV_{fuel}} \quad (31)$$

- Second law efficiency

The electrical exergy efficiency (ψ_{ele}), the thermal exergy efficiency ($\psi_{thermal}$) of the fuel cell are defined as Eq. 32 and 33, respectively. The fuel cell cogeneration exergy efficiency (ψ_{cog}) is shown in Eq. 34.

$$\psi_{ele} = \frac{\dot{W}_{APU}}{\dot{n}_{fuel} \dot{e}x_{fuel}} \quad (32)$$

$$\psi_{thermal} = \frac{\sum \left(1 - \frac{T_0}{T}\right) \dot{Q}}{\dot{n}_{fuel} \dot{e}x_{fuel}} \quad (33)$$

$$\psi_{cog} = \frac{\dot{W}_{APU} + \sum \left(1 - \frac{T_0}{T}\right) \dot{Q}}{\dot{n}_{fuel} \dot{e}x_{fuel}} \quad (34)$$

Efficiency based on First Law focuses its attention on reducing losses by treating all forms of energy as equal, whether mechanical or thermal energy. Exergy efficiency is generally lower than energy efficiency, due to the presence of process irreversibilities, which destroy part of the initial exergy. Nevertheless, the exergetic efficiency provides a more accurate understanding of system performance.

2. Case Study

For the purpose of this study, it is considered an Airbus A320 and its respective APU, a Honeywell 131-9A, this will be the APU used as reference when calculating the impact on weight, emissions and fuel consumption of the alternative APU. This gas turbine provides up to 300 kW when it is at full load (main engines start). In standard conditions the usage of the APU for the aircraft requirements is about 85 kW, through a generator up to 90/120 kVA, using the bleed air for pneumatic purposes. This means that there is enough energy available for other electrical purposes.

Following the concept of a more electric aircraft, the HT-PEMFC APU is designed to achieve a power demand of 250 kW during the entire flight envelope, which is a lot more than the gas turbine APU can provide. The system fuel is methane, requiring some extra components, to be converted into hydrogen. For the cathode side, ambient air is used as an oxidant. The fuel cell is configured to achieve the power goal. The proposed system displays a combination of power generation and waste heat recovery units. The Fuel Cell, Direct-Current inverter (DC), Gas Turbine, Compressor, Water Gas Shifting, Steam Reformer, and Pump units are used in power generation. Meanwhile, Heat Exchangers, Combustor and Heat Recovering Steam Generator (HRSG) are implemented to perform heat management in order to attain a better efficiency of the system. The simplified system layout is illustrated in Figure 1. In this system are presented five different flows: fuel, air, water, exhaust gases, and the cathode-off gases which correspond to the water vapor produced by the fuel cell and the amount of unused air.

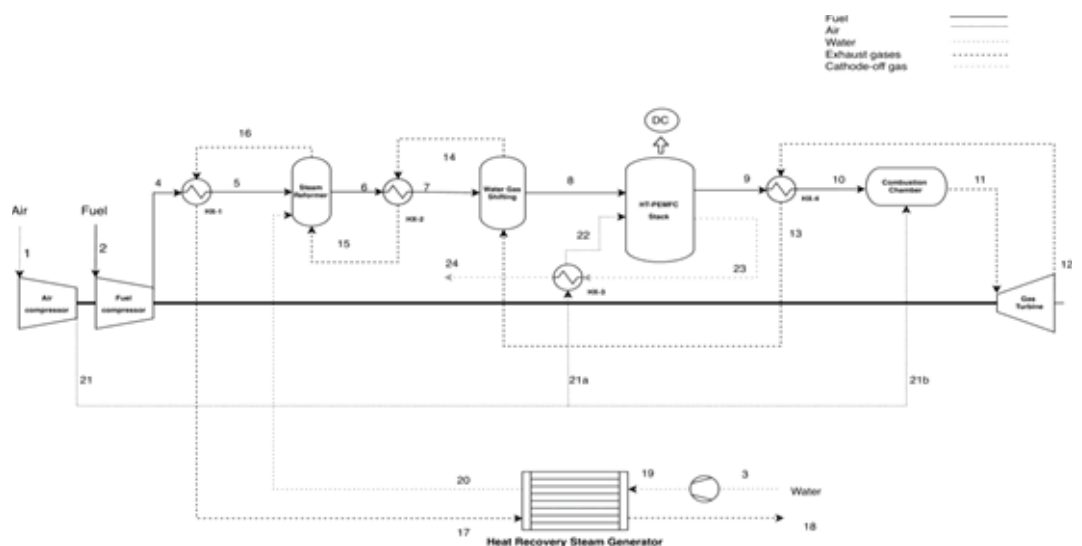


Figure 1: Proposed scheme for HT-PEMFC APU system layout.

Air enters the air compressor (1) before being supplied to the fuel cell and the combustor chamber. The air compressor is responsible for pressurizing the system on the ground where the pressure difference is constant and is turned off during the cruise phase. During the cruise phase, cabin air is used instead of ambient air, so the air compressor is no longer necessary. Fuel is also pressurized (2-4), but in this case, compression is required during all the flight envelope. When gas flows through a gas line it loses pressure due to the frictional resistance of the parts exposed to the gas. This pressure drop cannot be countered, so the fuel is pressurized to respond to those losses and to achieve the stack pressure. Methane is reformed in a steam reformer (5-6) and a water gas shifting (7-8). This way, a hydrogen-rich gas is fed to the fuel cell (8) to produce the electrical load required for the aircraft. A DC/DC converter converts the variable low-DC voltage output to usable DC power when required. Part of compressed air (21b) and unused fuel (10) from the anode are burned in the combustor to produce the required heat for the turbine to produce work. The turbine is responsible for providing the essential power to run both compressors and to produce the amount of expand the gases that transport the heat required for heat management.

Heat management in the integrated systems is carried out by heat exchangers (HXs) combined with the exhaust gases from the combustor chamber. The recovered heat is used to preheat the fuel (at HX-1 and HX-4) and air (at HX-3), to lower the temperature of the fuel from reformer to the shifting operating temperature (at HX-2), and to vaporize water for the methane steam reformer whereas retain the temperature of reformer at isothermal operation (at HRSG). In order to supply vapor water to the fuel processor, fresh water must be pressurized by a pump (3-19) to the required steam pressure for the HRSG. Gas flow from the recuperator has quality heat that can be used to generate saturated steam in the HRSG. The HRSG involves an economizer and an evaporator.

3. Results

3.1. Validation

The fuel cell characteristics obtained from the model and experimental results from Authayanun et al. at 150°C and different CO conditions are compared in Figure 2 [3]. As can be seen in Figure 2, there is an acceptable agreement between the model and the experimental results verifying the validity of the model with respect to temperature and CO concentration. Moreover, in order to verify the fuel processor model, the simulation results were compared with results from literature. Two sets of data were selected for

this purpose, experimental data by Di Bona et al. [4] and numerical data by Nomnqa et al. [5]. Figure 3 compares the simulation, experimental, and numerical results of the dry gas composition at the outlet of the WGS reactor. There is a god agreement between the simulation results from this work with the data sets.

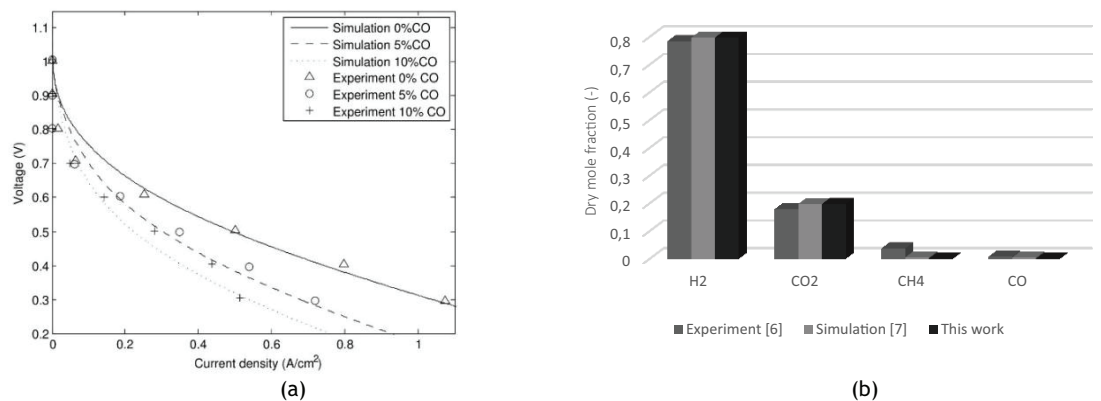


Figure 2: Validation of the voltage characteristics of the HT-PEMFC cell for 0%, 5% and 10% CO concentration at 150 °C (a) and validation of the experimental and numerical dry reformate gas from the fuel processor (b)

3.2. Pressure, Temperature and CO concentration analysis

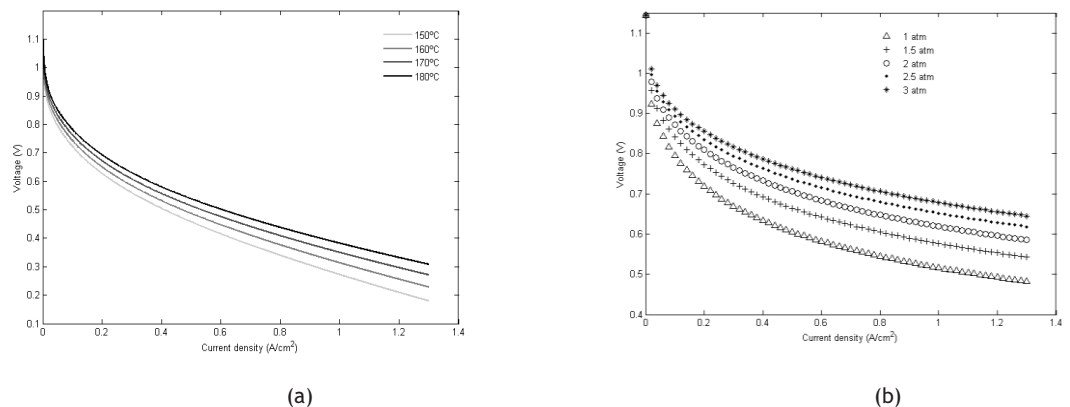


Figure 3: Fuel cell polarization curves voltage varying a) temperature and b) pressure.

Polarization curves are the most commonly used electrochemical method to characterize fuel cells, releasing essential information for the fuel cell analysis. Figure 3 (a) presents the polarization curves for temperatures of 150, 160, 170 and 180°C. From simulation results, is verified that the increment of temperature increases the performance of the cell voltage as shown in Figure 3 (b). This happens mainly due to an improvement in ionic conductivity with temperature and is also related to the faster kinetics and greater tolerance to the pollutants achieved at higher temperatures.

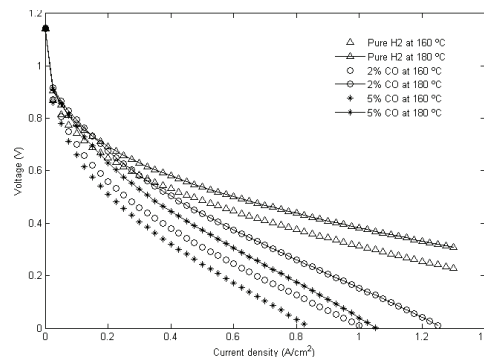


Figure 4: Fuel cell polarization curves at 160 °C and 180 °C for CO concentrations of 2% and 5% and pure hydrogen.

The efficiency of the system depends on the amount of carbon monoxide contained in the fuel when it reaches the HT-PEMFC since it can only handle small amounts of CO. Therefore, it is important to evaluate the percentage of CO contained in the reformed fuel to assess if it is detrimental to the cell. Figure 4 shows the behavior of the fuel cell when supplied with reformed fuel containing different CO concentrations (0%, 2% and 5%) and pure hydrogen for reference purposes. It can be stated that increasing CO concentrations result in the decrease of performance, although at low current densities this drop is almost nil and becomes more evident with the increase of current density (above 0.05 A/cm^2). Hence, HT-PEMFC operating on reformed fuel is ideally suited for low current densities as it shows a great CO tolerance, meanwhile pure hydrogen is favorable for high current densities operation. Although HT-PEMFC can operate with high amounts of CO, it is clear in Figure 4 how it starts to affect its performance when CO coverage is above 5%. In addition, tolerance to CO increases with HT-PEMFC operating temperature as demonstrated by Figure 4. At 160 °C, the fuel cell tolerance to 2% and 5% of CO is more sensitive than at 180 °C, as evidenced by the drop in cell voltage.

3.3. Design Operating Point

It is essential to select a design point to replace the APU gas turbine with a HT-PEMFC system. This design point represents the operation of a single cell that is the basis for dimensioning the fuel cell stack. The fuel cell stack is the power source of the APU system, so achieving a high-power density along with a high cell efficiency is critical. The maximum power density of the fuel cell increases linearly with temperature, which indicates the benefit of high-temperature operation, as shown in Figure 5.

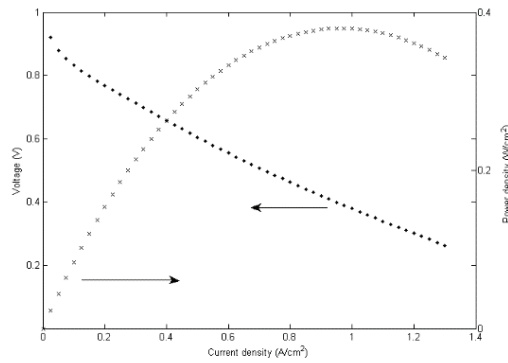


Figure 5: Fuel cell polarization curves at 160 °C and 180 °C for CO concentrations of 2% and 5% and pure hydrogen.

Table 1 shows the operating conditions and the product compositions of the fuel reforming and shifting processes. An S/C ratio of 3 and reformer temperature of 627 °C have a strong effect on the cell polarization curve, not only when the cell is operating at 180 °C but also at 150 °C. Table 1 presents the input parameters and the results for the stack dimension obtained from the MATLAB program.

TABLE 1: Fuel cell polarization curves at 160 °C and 180 °C for CO concentrations of 2% and 5% and pure hydrogen.

Parameters	Value	Unit
Ideal stack voltage	186	V
Number of cells in a module	333	
Module power density	126.5	W/cm ²
Module current	1426	A
Number of modules in a stack	6	
Stack heat generated	283	kW
Specific power	0.577	kW/kg
Cathode utilization	44.0	%

3.4. Exergy destruction

The major source of irreversibilities is the internal thermal energy exchange associated with high-temperature gradients caused by heat release in combustion reactions. These mechanisms are the Fuel Cell, the Combustion Chamber and the Steam Reformer. The heat exchangers and the HRSG are also components of high exergy destruction. The irreversibilities are due to the various phenomena, subject to the universal laws of thermodynamics, coupled with the natural degradation of materials and the increase of their disorder, where entropy plays an essential role. When analyzing the components

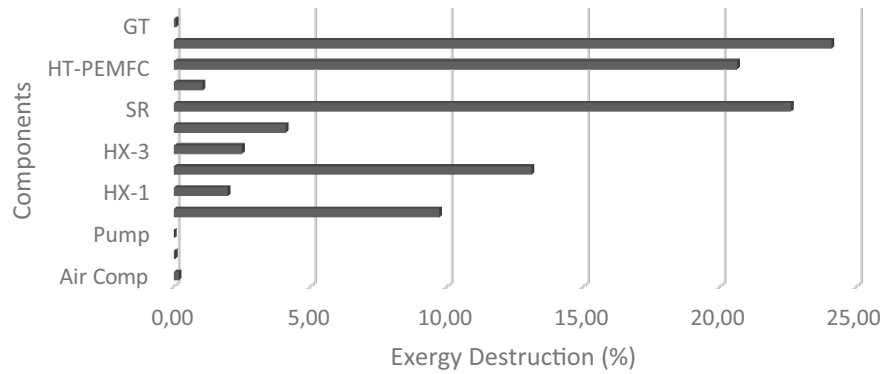


Figure 6: Exergy destruction quotient of each component of the HT-PEMFC system.

with the major irreversibility, and greater exergy losses, these may be the components where the efficiency of the components can be improved by the introduction of more efficient specific processes, alterations to the designs, reconfiguration of several components, using different materials.

3.5. Breakeven Weight

The total system weights 1115 kg, where the HT-PEMFC, the converter, and the HXs are key players in the weight of the HT-PEMFC APU. This corresponds to a weight increment of 854 kg (after adjusting for elimination of the APU and reduction in converter weight) when compared to the conventional gas turbine APU.

Figure 7 represents graphically the difference between the estimated weight impact for the fuel cell design point (0.56 V, 0.68 A/cm²) and the break-even weight is the estimated weight reduction required for saving fuel by increasing the efficiency of the system, which increases with the flight distance. The extent of weight reduction required is less for shorter flights.

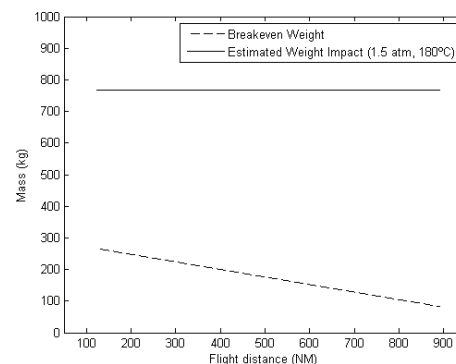


Figure 7: Plot comparing the estimated system weight in scoping calculation to the breakeven weight for 1.5 atm, 0.56 V/cell.

4. Conclusion

The best system performance was generated with an efficiency of 41.23% by a cell operating temperature of 180 °C and pressure of 1.5 atm. The heat recovery for cabin heating had the objective of increasing the efficiency of the system and producing the necessary energy for the aircraft, with 69.5% efficiency. The impact of the weight increment (854 kg) by installing the HT-PEMFC APU is canceled at the break-even point, where the weight increment for the heavier system is equal to the fuel saved due to its outstanding efficiency. The proposed system was validated through a thermodynamic balance model and, the fuel processor and the fuel cell mathematical models showed very good agreement with experimental data under various operating conditions. The exergetic method confirmed its usefulness in the analysis of energy systems. The major irreversibilities were generated by the fuel cell and the combustor chamber with an exergy destruction quotient of 19.71% and 23.04%, respectively. In conclusion, the application of fuel cells will continue to be an intriguing and vibrant area of research toward the ultimate and ambitious goal: a completely electric aircraft.

References

- [1] A. Anger, "Including aviation in the European emissions trading scheme: Impacts on the industry, CO₂ emissions and macroeconomic activity in the EU," *Journal of Air Transport Management*, vol. 16, no. 2, pp. 100–105, 2010.
- [2] D. Aili, H. A. Hjuler, J. O. Jensen, and Q. Li, *High Temperature Polymer Electrolyte Membrane Fuel Cells: Approaches, Status, and Perspectives*, 1986.
- [3] S. Authayanun, M. Mamlouk, and A. Arpornwichanop, "Maximizing the efficiency of a HT- PEMFC system integrated with glycerol reformer," *International Journal of Hydrogen Energy*, vol. 37, no. 8, pp. 6808–6817, 2012.
- [4] D. Di Bona, E. Jannelli, M. Minutillo, and A. Perna, "Investigations on the behaviour of 2 kW natural gas fuel processor," *International Journal of Hydrogen Energy*, vol. 36, no. 13, pp. 7763–7770, jul 2011.
- [5] M. Nomnqa, D. Ikhu-Omoregbe, and A. Rabiou, "Parametric analysis of a high temperature PEM fuel cell based microgeneration system," *International Journal of Chemical Engineering*, vol. 2016, 2016.